PTEP

Prog. Theor. Exp. Phys. **2012**, 03C006 (13 pages)
DOI: 10.1093/ptep/pts078

Beta-gamma spectroscopy at RIBF

Shunji Nishimura*

RIKEN Nishina Center, Wako, Saitama 351-0198, Japan
*E-mail: nishimu@ribf.riken.jp

Received October 11, 2012; Accepted November 14, 2012; Published December 11, 2012

β-decay spectroscopy is a powerful method of shedding light on the evolution of nuclear structure toward extreme neutron-to-proton ratios. This paper summarizes the experimental status of and plans for β-decay projects with new devices optimized for measurement of β-decay half-lives, β-delayed γ, β-delayed neutrons, and isomers using the new-generation Radioactive Isotope Beam Facility (RIBF) at RIKEN.

1. Introduction

The study of exotic nuclei is challenging and is expected to provide new features of the nuclear structure in extreme neutron-to-proton ratios. Recently, the possible weakening or disappearance of traditional shell closures and the appearance of new magic numbers have been discussed due to the new physics of weak binding and the theoretically expected role of tensor force in single-particle energies [1–4]. An enormous amount of experimental effort has also been devoted to this over the last two decades, finding some interesting features for shell evolution: the existence of the $N = 16$ shell closure [5], collapse of the $N = 20$ and 28 shell closures [6,7], the $N = 32$–34 subshell closure [8,9], and the possible emergence of the magic number $Z = 16$ [10]. Extension of the shell evolution study toward exotic and heavier regions becomes more challenging in the search for new phenomena.

The properties of very neutron-rich nuclei far from stability play an important role in the nucleosynthesis of heavy elements, where about half of the elements heavier than iron are explained as being produced in a rapid-neutron-capture process (r-process) nucleosynthesis [11]. r-process nucleosynthesis requires a high-density neutron environment to satisfy the condition of $(n, \gamma) \rightleftharpoons (\gamma, n)$ competition in a short time. However, its astronomical site and the mechanism are not fully understood [12,13]; a basic parameter of neutron-rich nuclei produced along the r-process path is required. For example, β-decay half-lives are responsible for the process speed and abundance, mass (Q_β) determine the location of the r-process path, and neutron-emission probabilities (P_n) will change the abundance pattern in the freeze-out time. The properties of these important r-process nuclei are, however, not known due to their limited production yield in the laboratory. Therefore, a new-generation heavy ion facility with high primary ion beam intensities is desired.

2. Decay spectroscopy: cases from physics

2.1. *Shell-structure evolution around doubly magic nuclei*

Spectroscopic study of doubly magic nuclei such as ^{48,78}Ni and ^{100,132}Sn provide important benchmarks for the shell structure and their few valence particle neighbors. A number of

experimental efforts have been devoted to those nuclei over recent decades at world-wide frontier facilities [14–16].

Nickel isotopes (Ni): Nickel is expected to have three doubly magic nuclei (^{48}Ni, ^{56}Ni, and ^{78}Ni). Testing the magicity of ^{78}Ni and ^{48}Ni is one of most attractive subjects, which has mainly been discussed in theory. Four ^{48}Ni and three ^{78}Ni nuclei were reported for the first time using fragmentation of a nickel beam (^{58}Ni) and the in-flight fission of a uranium beam (^{238}U), respectively [14,17]. In particular, ^{78}Ni has the largest neutron-to-proton ratio value, and is thus one of the best candidates to study the evolution of nuclear structure far from the valley of stability. ^{78}Ni is also considered to be a key nucleus in r-process nucleosynthesis, where its β-decay half-life will affect the initial condition of r-process nucleosynthesis [18]. The β-decay half-life of ^{78}Ni was measured for the first time at MSU and found to be shorter than the predicted value, although it has large uncertainties, mainly due to statistical errors ($T_{1/2} = 110^{+100}_{-60}$ ms) [15]. In November 2012, β-decay spectroscopy of the ^{78}Ni region was performed using a high-intensity uranium beam at RIBF. New results for β-decay half-lives and the β-delayed γ and possible isomeric states around ^{78}Ni are foreseen to appear in the near future.

Tin isotopes (Sn): The doubly magic nucleus ^{100}Sn on $Z = 50$ and $N = 50$ is found to have the smallest log(ft) value of $2.62^{+0.13}_{-0.11}$ [19]. Higher end-point energy precision in the decay of ^{100}Sn is, however, desired to improve the B_{GT} value. A high-precision measurement of the end-point energy requires one order higher statistics of ^{100}Sn, which can be obtained using fragmentation of a ^{124}Xe beam at an intensity above 20 pnA at RIBF. In addition, the search for the elusive isomeric 6^+ state would be possible if the lifetime of the state is sufficiently long in excited states in ^{100}Sn. Measurement of the β-decay half-life of ^{99}Sn and confirmation of the possible drip-line nucleus ^{98}Sn also provide systematic shell evolution beyond ^{100}Sn.

Shell quenching: The issue of the occurrence of shell quenching in connection with astrophysical scenarios has been widely debated, in particular for $N = 82$ around the r-process waiting points [20,21]. One of the highest intensities proved at RIBF is the neutron-rich region around $N = 82$, where thirteen ^{128}Pd particles were produced for the first time [22]. The β-decay half-lives and possible isomer around ^{128}Pd will reveal important clues to the $N = 82$ shell closure and possible quenching due to a softening of the neutron potential [1,23,24] or increased excitation of neutrons into orbitals beyond $N = 82$ leading to deformation [2], where those scenarios are introduced to explain the deficiency below the second peak r-process abundance. Similarly, the transition region of mass $A = 180 \sim 190$ between deformed and spherical structures will strongly affect the suppression of the abundance before the third peak $A = 195$ due to the long-range correlations for nuclear masses [25].

2.2. Deformation

Nuclei exhibit a wide variation of nuclear structural properties [26], including well-deformed prolate shapes with rotational band structures [27], and shape transitions across isotopic and isotonic chains. For example, it is rare for nuclear ground states to have oblate deformations, and recent observations of nuclides in the $A = 80$ and 190 regions near the proton drip line have led to renewed interest in the stability of oblate shapes [28,29]. Such shape isomers are expected to occur in the neutron-deficient nuclei around $A = 80$, the neutron-rich $A = 100$ region, and neutron-deficient Pb, taking account of axial asymmetry [30].

There are various experimental approaches to discuss the deformation of nuclei. Recently, a new feature of isotopes has shown sudden and intense deformation in the ^{96,97}Kr region and systematic

overestimation of binding energies around the mass $A = 110$ region [31,32]. Thus, it is interesting to measure the end-point energies of β-rays in the decay experiment. Another approach is to measure the first two yrast states of even–even nuclei: the energy of the first 2^+ state and the ratio $R_{4/2} \equiv E(4_1^+)/E(2_1^+)$ of the first two yrast states. Such a systematic trend in the low-lying levels and the ratios has been discussed and provides some evidence for the sudden onset of deformation [33].

2.3. Nuclear astrophysics

β-decay-related information, such as β-decay half-lives, β-delayed γ and β-delayed neutron-emission probabilities, and nuclear masses (Q_β), is known to play an important role in the r-process. The β-decay half-lives and β-delayed neutron branching around ^{78}Ni isotopes were measured and their impacts on the r-process abundance were studied by comparing the theoretical predictions [15,34–36]. The accessible nuclei along the r-process path are, however, limited in the neutron number $N = 50$–82 region, and reduced to almost nothing beyond mass $A \geq 140$ due to the difficulty of producing these isotopes in the laboratory.

In this paper, the experimental approach of studying β-decay and the associated β-delayed γ-decay and isomer will be reported using various devices dedicated to decay spectroscopy at RIBF.

3. Experiments at RIBF

Recently, the Radioactive Isotope Beam Factory (RIBF) at RIKEN Nishina Center (RNC) has been completed and has provided beams of 345 MeV/nucleon since 2006 [37]. The scientific program of exploring exotic nuclei using a high-intensity uranium beam has successfully demonstrated its great potential of producing very neutron-rich nuclei by means of the in-flight fission method combined with the help of the large acceptance of the transportation beam-line (BigRIPS) [22,38]. In a series of new isotope search programs, more than 45 new isotopes were discovered with a uranium beam intensity of 0.2 pnA at 345 MeV/nucleon. The goal of uranium beam intensity is 1 pμA, corresponding to a factor of 5×10^3 higher than what we achieved in 2008. The Zero-Degree spectrometer (ZDS) after BigRIPS was constructed to perform additional particle identification with a longer time-of-flight path. A schematic drawing of BigRIPS and the ZDS is shown in Fig. 1.

The first decay spectroscopy experiment was conducted in 2009 using 0.1–0.3 pnA of a uranium beam. The first stage of BigRIPS was employed for selection and purification of the produced

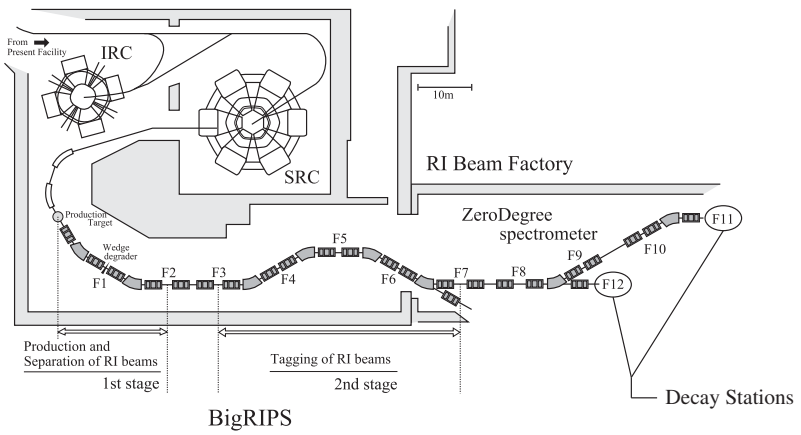

Fig. 1. Overview of the RIBF facility. The radioactive ion beams were produced and separated with BigRIPS and transported to the β-decay station at focal points F11 or F12.

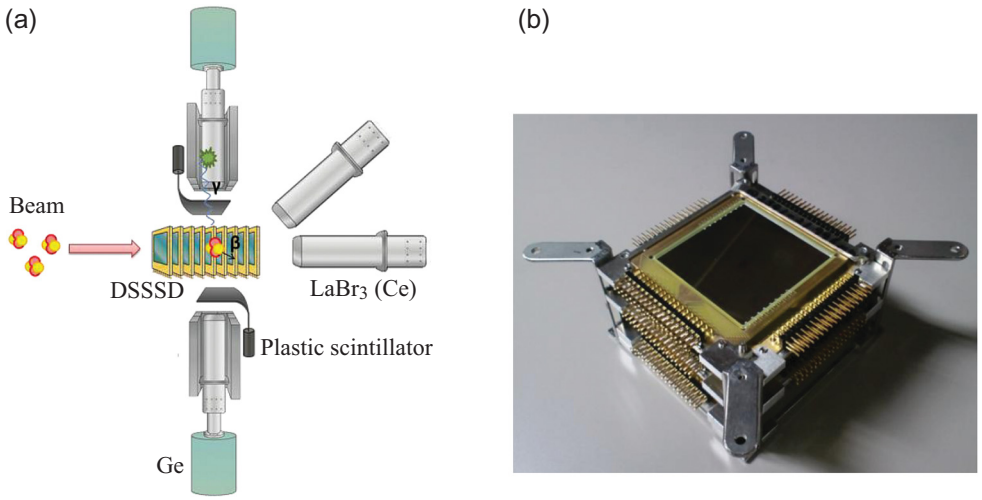

Fig. 2. (a) Experimental setup performed in 2009 at RIBF. The produced isotopes were stopped in double-sided silicon-strip detectors (DSSSD). γ-rays were detected by four Compton-suppressed clover-type Ge detectors arranged around the DSSSDs in a close geometry. (b) Nine stack of DSSSDs installed in the vacuum chamber to stop the produced isotopes. The β-rays emitted from the radioactive isotopes were detected with an efficiency of 40–80%.

isotopes by the $B\rho - \Delta E - B\rho$ method, while in the second stage the particles were identified using $B\rho - \Delta E$ and time-of-flight (TOF) information. The secondary beam was slowed down by means of an aluminum degrader and stopped in an active silicon detector for half-lives and β-delayed γ-ray measurements. An independent data acquisition system was introduced for the first time to achieve parallel data transfer for the BigRIPS/ZDS, β-ray detectors, and γ-ray detectors. A schematic view of the experimental setup and the appearance of the silicon detectors are shown in Fig. 2. The silicon detectors consist of nine double-sided silicon-strip detectors (DSSSD: Micron Model W1-1000) segmented with 16 strips in the horizontal and vertical axes as a position-sensitive β-counting system. A freezer system was introduced to cool the DSSSDs down to -25 degrees to be operational for long-term experiments with minimum leakage current. The produced isotopes were implanted in the DSSSDs and their energy losses deposited in one of every two DSSSDs (second, fourth, sixth, and eighth) were measured for confirmation of the implantation position on an event-by-event basis. The β-counting system was surrounded by four clover-type germanium detectors to measure γ-rays from isomeric states and the excited states of the daughter nucleus after β-decay.

The detection efficiency of β-rays varies as a function of implantation depth in each DSSSD. It reaches a minimum on the surface of the DSSSD with 40% and a maximum in the middle of the DSSSD with better than 80%. The full-energy peak efficiency at 300 keV was 3% for all the γ-ray detectors. A shape evolution at proton number $Z = 40$ was investigated in neutron numbers $N = 64$ to 68. The results indicate a minimum excitation energy of the first 2^+ state at $N = 64$ and a gradual increase up to the neutron numbers $N = 68$ [39], indicating some hints of higher excited state at $N = 70$ ^{110}Zr. The low-lying levels of ^{109}Nb were also investigated in both the ^{109}Nb isomer itself and β-delayed γ-rays of ^{109}Zr. Although confirmation of the quadrupole moments and g-factors is required, the identified isomeric state at an excitation energy of 313 keV, which is far below the pairing gap energies for both protons and neutrons, could be an oblate-deformed state [40].

In this experiment, new half-lives of very neutron-rich Kr–Tc on the boundary of the r-process have been also deduced successfully [41]. The 38 β-decay half-life parameters enable us to extract new

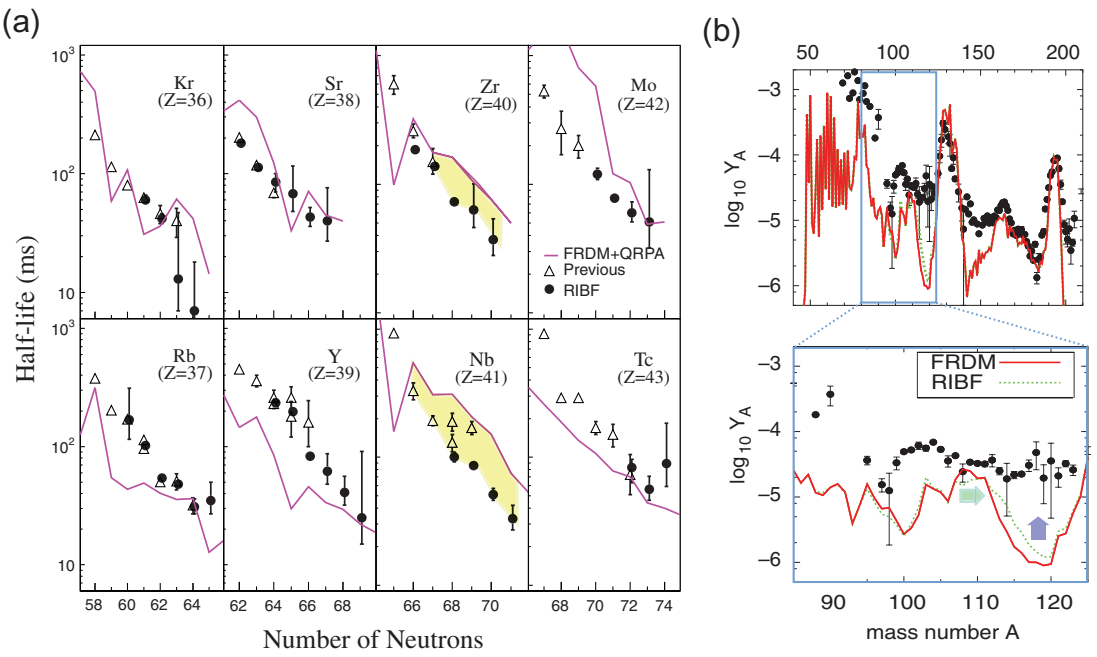

Fig. 3. (a) β-decay half-lives for Kr–Tc isotopes as a function of neutron number. Filled circles and open triangles correspond to the RIBF data and previous work, respectively. The solid line is the FRDM+QRPA prediction. (b) Final abundance distributions of r-process elements using the FRDM parameters (solid line) and replaced half-life data from RIBF (dotted line) from Ref. [44].

systematics that theoretical prediction (FRDM+QRPA) shows better agreement for more neutron-rich isotopes for Kr, Rb, Sr, Y, Mo, and Tc isotopes, but seems to overestimate for that of Zr and Nb isotopes by a factor of 2 or more [42,43]. The impact of these newly obtained β-decay half-lives was studied with the help of an r-process network calculation. The results show the recovery of the underestimation below the second peak region, the $A = 110$–120 region, by a factor of 2.5 due to the fast β-decay flow below $A = 110$. However, the effects are not enough to explain the overproduction in the solar system relative to the theoretical calculations [44]. The systematic underestimation of the half-lives in the mass $A = 110$ region suggests a possible underestimation of $\Delta Q_\beta = 1\,MeV$ in the standard theoretical model (FRDM). In future, a high-precision mass measurement of Zr and Nb isotopes beyond $N = 70$ is desired to confirm the reasons, where possible subshell closure is predicted [45].

In the next section, the devices developed for decay spectroscopy at RIBF will be introduced: WAS3ABi and CAITEN for β-ray detection, EURICA for γ-ray detection, and the ^{3}He detector and plastic scintillation detector for neutron detection.

4. High-segmentation β-counting system: WAS3ABi

An active stopper with position sensitivity provides a great opportunity to perform β-delayed γ spectroscopy and in the cocktail beam environment. A new β-counting system, WAS3ABi (wide-range active silicon-strip stopper array for beta and ion detection), with 19 200 segmentations, has been developed to maximize the physics outputs in conjunction with the highest-efficiency γ-ray detector at RIBF. The double-sided silicon-strip detectors (DSSSD: Canberra PF-CT-CD 60 × 40 × 1 mm^3), designed for the SIMBA detector [46], are employed with segmentation of 60 1-mm wide strips in the horizontal and 40 1-mm wide strips in the vertical directions, respectively. WAS3ABi

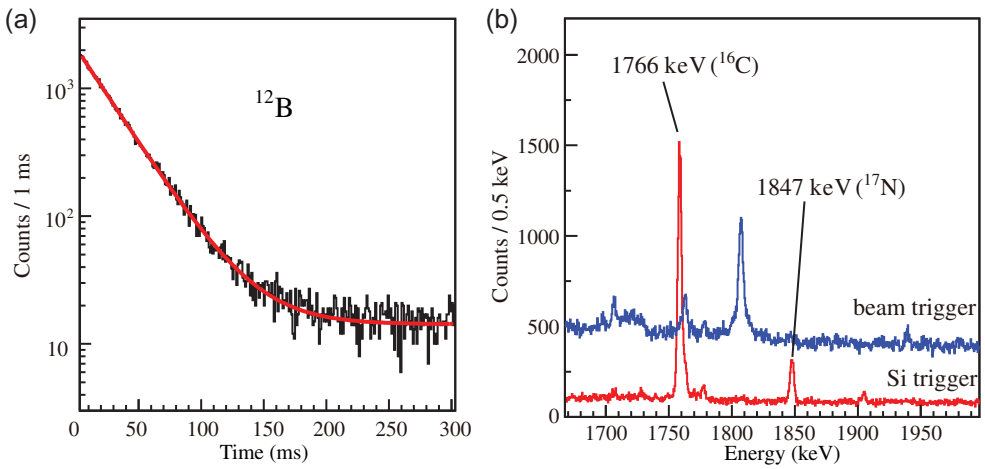

Fig. 4. (a) Time distribution of β-decay events correlated with an implanted ^{12}B nuclide. Fit (line) takes into account an exponential decay and a constant background. (b) Selection of the γ spectra gated on implantation of ^{12}B and gated on their subsequent β decays. The peaks labeled with their energies are β-delayed γ-rays.

consists of eight layers of DSSSDs and it is designed to stop all the fission products of the uranium beam with large momentum spread. A thick scintillation detector ($40 \times 60\,\mathrm{mm}^2$, $40\,\mathrm{mm}^t$) mounted downstream of WAS3ABi will be used to reject light particles, and the fast timing of β-decay and possible Q_β values can be obtained.

A decay curve is constructed for each nuclide by measuring the correlation between heavy-ion implantation and subsequent β particles detected within the same pad and the same DSSSD layer. The uncertainty of β-decay half-life strongly depends on the detection efficiency of low-energy β-rays, background, the half-lives of daughter and granddaughter, and β-delayed emission branches (P_n). Because of the more severe problem for nuclei with a limited number of statistics and higher P_n values for very neutron-rich nuclei, a new readout system for WAS3ABi was developed for high-efficiency β-ray measurements, aiming to achieve a precise half-life measurement with twice the detection efficiency of β-rays (80%) with an energy threshold below 20–30 keV [47]. The commissioning of the readout electronics of WAS3ABi was performed in conjunction with the BigRIPS/ZDS spectrometer.

5. EUROBALL RIKEN cluster array: EURICA

A new project, EURICA (EUROBALL RIKEN Cluster Array), which proposes to utilize the EUROBALL cluster detectors for an experimental campaign at the RIBF, was approved and launched in 2011 [48]. EURICA aims to conduct isomer and β-delayed γ-ray spectroscopy of several hundred nuclei far from stability. EURICA consists of 12 seven-element cluster germanium detectors [49], and was formerly used as RISING at GSI [50,51]; it has been installed at the F11 focal point at RIBF together with its support structure. In total, 84 cluster capsules are arranged to form a spherical shape with an inner diameter of 38 cm (see Fig. 5). The EURICA cluster detectors are mounted on a 4 m long rail system to be able to open two independent hemispherical parts for the installation of an active beam stopper for the β-decay experiment. Each energy signal from the cluster capsule is fed into fully digital electronics using DGF-4C modules from XIA. An energy resolution of better than 3 keV at $E_\gamma = 1.3$ MeV was confirmed with an expected photo-peak efficiency of about 15% at $E_\gamma = 662$ keV. The advantage of EURICA is that it can study the low-lying states of nuclei with a detection efficiency one order of magnitude higher than for single γ-ray detection, i.e., two orders of

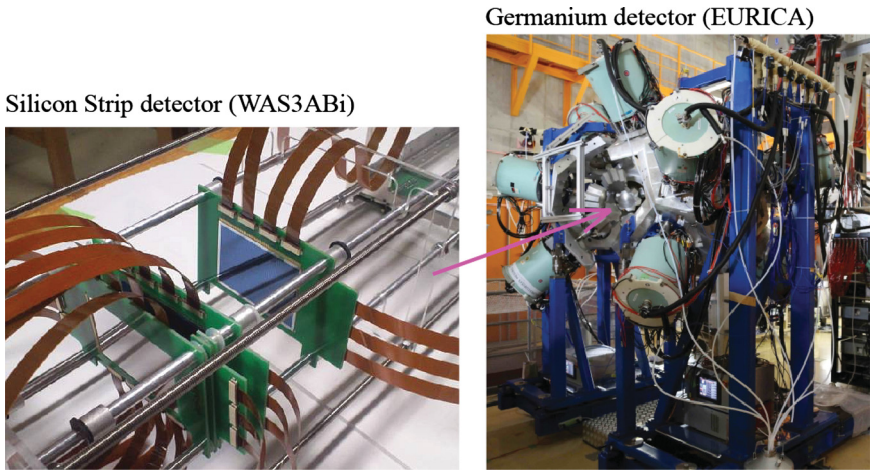

Fig. 5. The EURICA setup, consisting of double-sided silicon-strip detectors (WAS3ABi) and 12 Euroball cluster detectors (EURICA). The device has been installed at the last focal point of the BigRIPS/ZDS spectrometer for the stopped-beam campaign at RIBF.

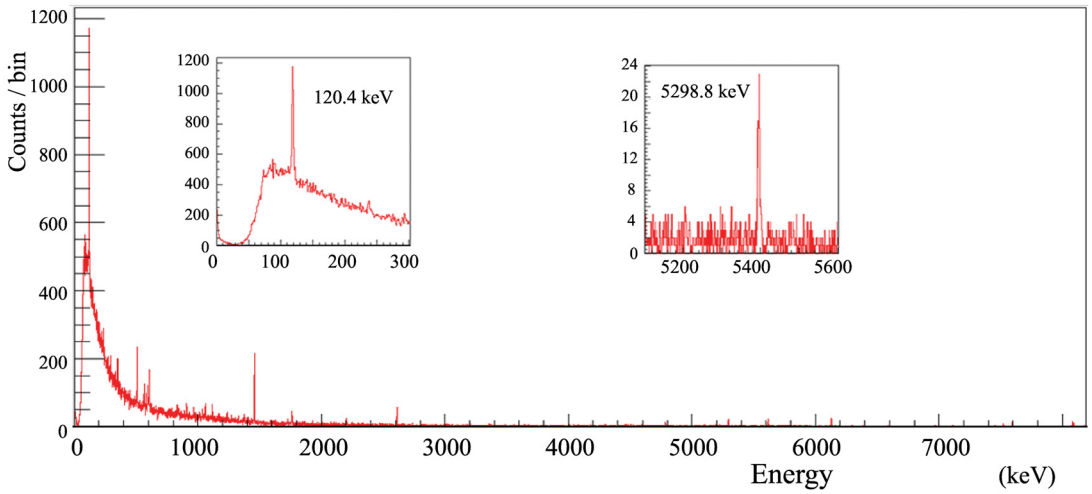

Fig. 6. Online spectrum from the EURICA cluster array with four hours of data collection. The insets show the isomeric decay $0^- \rightarrow 2^-$ transition in ^{16}N and β-delayed γ of ^{15}N with energies of 120.42 keV and 5298.8 keV, respectively.

magnitude higher for $\gamma\gamma$-coincidence, compared to the previous β-decay spectroscopy conducted at RIBF [39,40,52].

The commissioning of the cluster detectors was carried out to verify their required performance for energy and lifetime measurements of isomeric states and β-delayed γ-rays coincident with the β-decay trigger. In total, 4 days of beam time were devoted to using ^{18}O as a primary beam at energies of 230 MeV/nucleon. Figure 6 shows the $0^- \rightarrow 2^-$ transition in ^{16}N confirmed online for isomeric detection, with an energy of 120.42 keV and a lifetime of 5.25 μs, where an ^{152}Eu source was used for its energy calibration. γ-rays following the β-decay of implanted nuclei could be clearly detected. For example, γ-rays at energies of 5298.8 keV for $1/2^+$ to $1/2^-$ in ^{15}N were clearly seen at their correct energies.

In June 2012, the first scientific program of EURICA, aiming to study isomeric states and β-delayed γ-rays around ^{98}In, ^{95,96}Cd, and ^{94}Ag, was successfully performed. A primary beam of ^{124}Xe was used to produce these exotic nuclei at a maximum beam intensity of about 27 pnA.

Many physics cases, proposed as experimental campaigns for EURICA, will be carried out at RIKEN, where ^{48}Ca, ^{78}Kr, ^{124}Xe, and ^{238}U are expected as primary beams with expected intensities of 200, 20, 10, and 5 pnA, respectively. For example, the first EURICA campaign with a ^{238}U beam was conducted in 2012 with twenty times higher intensity ($I \sim 8$ pnA) compared to the previous β-decay experiment in 2009. Additional γ-ray detectors such as $LaBr_3$(Ce) and NaI(Tl) detectors for γ-rays, or liquid scintillation detectors for neutron measurement, can be installed in the three empty slots of the cluster detectors. Series of EURICA campaigns are planned to perform $\beta\gamma$ spectroscopy in neutron-rich and proton-rich nuclei by at least December 2014.

6. Super-segmented plastic scintillation detector: CAITEN

At low-energy ISOL facilities, a fast β-counting system, consisting of a thin passive tape transporting system and a plastic scintillation detector, has been applied to β-decay spectroscopy, such as high-precision half-life measurement [53], β-delayed neutron measurement by the time-of-flight (TOF) method [54], and nanosecond isomeric lifetime measurement [55–58]. Application of such a fast timing detector at a fragmentation beam facility under cocktail beam environment is challenging, but will be a breakthrough for extending new physics cases of decay spectroscopy. A novel detector consisting of a segmented plastic scintillation detector has been developed to cover the additional physics case of β-decay spectroscopy with fast timing at RIBF. A prototype detector system with rotating multi-layer passive plates was prepared and can be used to apply the β-decay spectroscopy of long-lived isotopes due to the limited time of transporting the isotopes in the detector section ($\sim$50 ms) [59]. Its dead-time, however, becomes more and more critical for nuclei far from stability with shorter lifetimes.

A novel β-counting system, CAITEN (cylindrical active implantation target for exotic nuclei), has been constructed based on the new idea of an active-scintillator transporting-detector system as a complementary device to the DSSSD, or the tape transporting system. The CAITEN consists of a position-sensitive photomultiplier tube (PSPMT) array and a cylindrically arranged rotating plastic scintillator (TPS: ϕ 500 mm $\times$ 1000 mm, 20 mm^t) as an active implantation target to stop the isotopes. The primary goal of CAITEN is to perform high-precision β-decay spectroscopy of rare isotopes, where application of the DSSSD becomes unsuitable due to its radiation damage, slow timing response, higher β-counting rate from the accumulated daughter nuclei, and pile-up of incident particles and possible light-particles under a higher-intensity secondary beam. The CAITEN apparatus is shown in Fig. 7(a).

The TPS consists of 4×10^4 scintillator pixels (EN-208: $6 \times 6 \times 20$ mm^3) glued onto a cylindrical plastic tube (outside: ϕ 500 mm $\times$ 5 mm thickness) and this arrangement is mounted onto two rotating rims. The dimensions of one plastic scintillation bar are 24.5 mm $\times$ 498 mm with a pitch of 6 mm ($4 \times 83 = 332$ pixels). Al plates (0.4 mm^t) were inserted between the pixels for reflection and isolation of the scintillation light. A cutter depth of 15 mm is used. The remaining 5 mm is used to fix the pixels. In total, 128 scintillation bars are attached to acrylic tubes (ϕ 500 mm $\times$ 1000 mm) to obtain a smooth arrangement. The surface of the TPS is finally covered by 15 μm of Al foil to reflect the scintillation light back towards the inner direction, where the PSPMTs are arranged to reconstruct the profile of the scintillation light. The CAITEN moves the TPS vertically at the beam height (170 cm $\pm$ 50 cm) synchronized together with a rotating motion at a speed of $0 \sim 60$ rpm by a

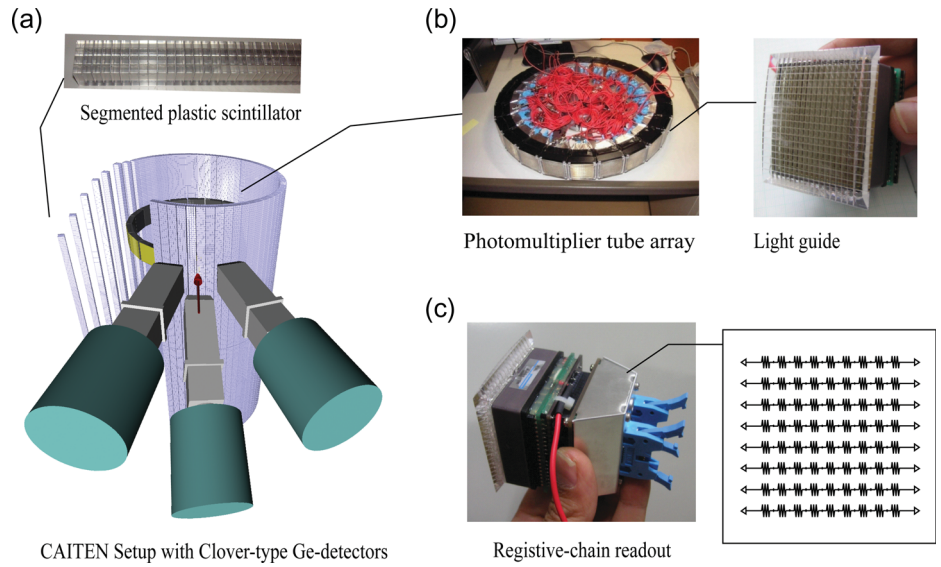

Fig. 7. (a) Segmented plastic scintillators. (b) Position-sensitive photomultiplier tube array. (c) Resistive channel readout of the PSPMTs.

programmable sequencer system. This idea is similar to the tape transportation system: to reduce the density of non-associated decay events from the previously implanted nuclei remaining in the TPS pixels. The adequate scintillator thickness of 20 mm helps us to stop energetic isotopes with a wider momentum spread, where the usual tape transportation system is not applicable at the RIBF.

Twenty-four flat-panel-type multi-anode photomultiplier tubes (Hamamatsu H8500) were employed as PSPMTs to reconstruct the positions and timings of both ion-implantation and β-decay. The photomultiplier tubes, H8500, have 64 pads of anode pixels arranged in an 8×8 matrix for the position measurement of the light. The last-dynode signals from the PSPMTs were used for the trigger. The emitted scintillation light from pixel scintillators was transferred to the PSPMT efficiently using a segmented-light-guide attached to each PSPMT (see Fig. 7(b)). The curvature of the light-guide with a 240 mm radius is designed to fit the inner TPS surface with a constant air-gap of about 3–4 mm to achieve the position resolution $\sigma_{\mathrm{pos}} \leq 4$ mm. A slow-response plastic scintillation material (EJ-240) was selected instead of Lucite for the light-guide material in the beam-line PSPMTs as photoswitch detectors to reject events of ions passing through the TPS.

A feasibility study of CAITEN was performed by implanting a cocktail beam in the TPS at a high implantation rate of about 10^3 particles per second. The secondary cocktail beam produced by projectile fragmentation of a 345 AMeV ^{48}Ca primary beam was primarily used for in-beam γ spectroscopy at the F8 focal point, where the secondary target was installed [60]. The isotopes transported from the F8 to F11 focal points were implanted in the CAITEN system. β-decay half-lives of very neutron-rich ^{29}F, ^{30}Ne, ^{31}Na, ^{35,36}Mg, and ^{37}Al isotopes were deduced by associating β-rays with each unambiguously identified isotope on the same scintillator-pixel, event-by-event basis. Figure 8(a) shows the particle identification of the ^{30}Ne setting and the significantly high statistic β-decay curve of ^{30}Ne. High-statistics γ-ray spectra, obtained using three clover-type germanium detectors in coincidence with the β-decays of those neutron-rich nuclei, shows γ-ray spectra results consistent with those obtained in previous work [61]. In addition, β-delayed γ-rays were measured in neutron-rich ^{37,38}Si for the first time, proving its capability of identifying the excited states [62,63].

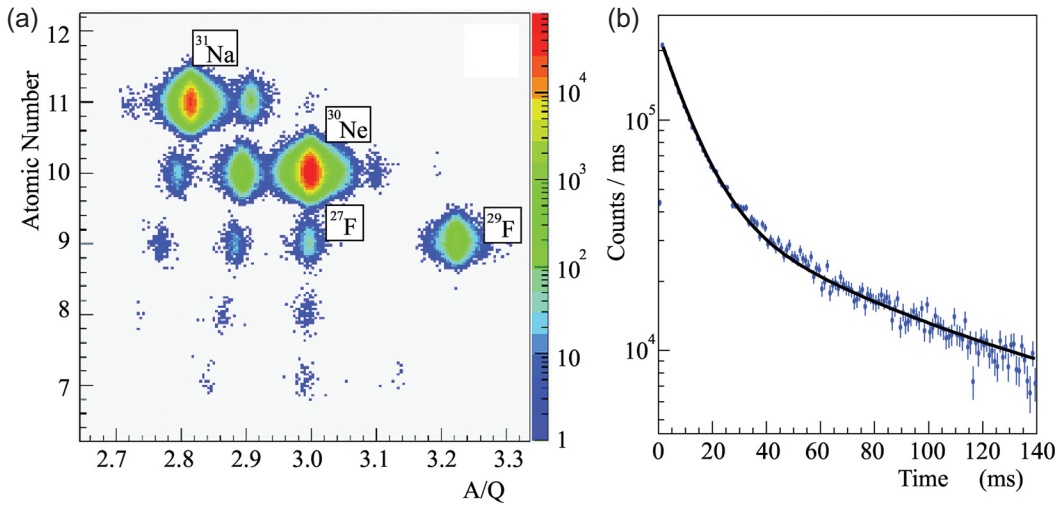

Fig. 8. (a) Particle identification performed in the ZDS beam-line. (b) β-decay curve of ^{30}Ne reconstructed in CAITEN.

The half-life of the nuclei was deduced from the time correlation between the implantation time of the identified fragments in the active catcher and the subsequent β-decay (see Fig. 8(b)).

In future, CAITEN will be employed to survey very neutron-rich nuclei and proton-rich nuclei together with the aim of performing new isotope search experiments with a relatively wider isotope coverage [22]. Large $LaBr_3$(Ce) detectors will be installed inside the TPS for fast γ-decay measurements. In addition to the clover-type germanium detectors, large scintillation hodoscopes will be installed to measure β-delayed neutrons using the time-of-flight method.

6.1. β-delayed neutron emission

β-delayed neutron emission is expected to be an essential process in very neutron-rich nuclei, where β-decay with more than one neutron emission is expected, due to decay proceeding to states above the neutron-separation energy (S_n). The gloss parameters of half-lives and β-delayed neutron-emission probability (P_n) are expected to be different with Gamow–Teller and first-forbidden transitions [64]. Therefore, the measured half-lives ($T_{1/2}$) and β-delayed neutron-emission probabilities (P_n) are expected to provide some probes into the nuclear structure of β-decay daughter nuclei.

Two experimental approaches for measuring β-delayed neutrons are planned at RIBF. One is an application of high-detection efficiency neutron detectors consisting of ^{3}He long counters and moderators to deduce the β-delayed neutron emission probability (P_n), as shown in Fig. 9(a). Another is the spectroscopic measurement of β-delayed neutrons using scintillation counters, where the energies of the emitted neutrons are deduced by the time-of-flight method [54]. Multiple layers of plastic scintillators and two position-sensitive photomultiplier tubes on both sides will enable us to measure the precise time-of-flight with additional information on the interaction point in depth. The prototype detectors were tested in conjunction with the fast β-counting system, CAITEN.

7. Summary

RIBF has started to provide the world's highest beam intensity for nuclei far from stability. A study of the decay properties of nuclei at the frontier of the exotic region can be achieved by satisfying all the necessary technical requirements: sufficient production yield of isotopes with high- intensity accelerators, a large-acceptance beam-line—BigRIPS—with particle identification capability, and

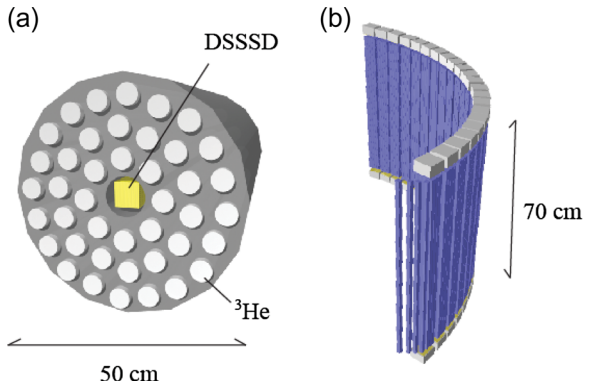

Fig. 9. (a) High-efficiency neutron detector consisting of ^{3}He long counters and moderators. (b) High-resolution time-of-flight detectors consisting of multiple-layer scintillation bars and position-sensitive photomultiplier tubes.

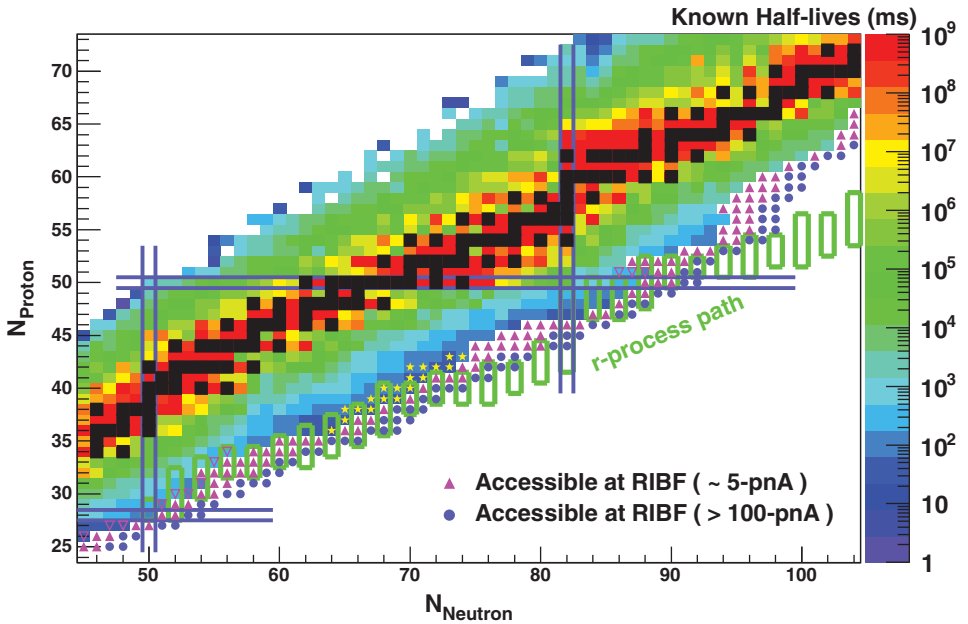

Fig. 10. Nuclear chart with nuclei with half-lives and the expected classical r-process path [65]. The color indicates the half-lives of each nucleus. The filled triangles and filled circles correspond to the regions of new half-lives expected using a uranium beam at intensities of 5 pnA and more than 100 pnA, respectively.

high-resolution and precision detection systems optimized for their facilities. Scientific programs related to decay spectroscopy have begun, aiming to measure β-decay half-lives and β-delayed γ-rays and isomers.

In the coming decade, several hundred unknown isotopes will be analyzed at RIBF using spectroscopy in order to glean insights about nuclear shell evolution, the appearance and disappearance of magicity, shape evolution in mid-shell regions, and the mystery of r-process nucleosynthesis. Figure 10 shows a nuclear chart with filled areas and boxes corresponding to nuclei with known half-lives and the expected classical r-process path, respectively [65]. At RIBF, several hundred neutron-rich nuclei on the r-process path will be accessible in the coming decades and their experimentally obtained gross parameters are expected to improve the prediction power of the theories.

One of the primary subjects is to study the shapes and yield of the first, second, and third abundance peaks (masses around $A = 80$, 130, and 195), where the important second peak element, tellurium, has recently started to be observed in astronomy [66,67]. The β-decay of neutron-rich nuclei between the second and third peaks (mass $A = 150$–180), which plays an important role in the synthesis of the rare-earth peak in freeze-out time, will be studied [68] in the future.

Acknowledgements

The decay spectroscopy experiments were carried out at RIBF, operated by the RIKEN Nishina Center, RIKEN and CNS, University of Tokyo. This work was supported in part by KAKENHI (19340074), RIKEN Presidents Fund (2005), and JSPS (22·00201). We are grateful to the EUROBALL Owners Committee for the loan of germanium detectors and the PreSpec Collaboration for the use of the readout electronics for the cluster detectors. Part of WAS3ABi was supported by the RISP Project at IBS. The authors thank the RIBF decay collaborators for their support on the decay experiments conducted at RIBF.

References

[1] J. Dobaczewski, I. Hamamoto, W. Nazarewicz, and J.A. Sheikh, Phys. Rev. Lett. **72**, 981 (1994).
[2] H. Grawe et al., Nucl. Phys. A **704**, 211c (2002).
[3] T. Otsuka, T. Suzuki, R. Fujimoto, T. Matsuo, D. Abe, H. Grawe, and Y. Akaishi, Acta Phys. Pol. **36**, 1213 (2005).
[4] T. Otsuka, T. Suzuki, J.D. Holt, A. Schwenk, and Y. Akaishi, Phys. Rev. Lett. **105**, 032501 (2010).
[5] A.Ozawa et al., Phys. Rev. Lett. **84**, 5493 (2000).
[6] T. Motobayashi et al., Phys. Lett. B **346**, 9 (1995).
[7] B. Bastin et al., Phys. Rev. Lett. **99**, 022503 (2007).
[8] A. Gade et al., Phys. Rev. C **74**, 021302 (2006).
[9] H. L. Crawford et al., Phys. Rev. C **82**, 014311 (2010).
[10] Y. Togano et al., Phys. Rev. Lett. **108**, 222501 (2012).
[11] E. M. Burbidge et al., Rev. Mod. Phys. **29**, 547 (1957).
[12] A. Burrows et al., New Astron. Rev. **50**, 487 (2006).
[13] S. Rosswog et al., Astron. Astrophys. **341**, 499 (1999).
[14] B. Blank et al., Phys. Rev. Lett. **84**, 1116 (2000).
[15] P. T. Hosmer et al., Phys. Rev. Lett. **94**, 112501 (2005).
[16] D. Bazin et al., Phys. Rev. Lett. **101**, 252501 (2008).
[17] M. Bernas et al., Phys. Lett. B **415**, 111 (1997).
[18] P. Hosmer et al., Phys. Rev. C **82**, 025806 (2010).
[19] C. B. Hinke et al., Nature **486**, 341 (2012).
[20] I. Dillmann et al., Phys. Rev. Lett. **91**, 162503 (2003).
[21] A. Jungclaus et al., Phys. Rev. Lett. **99**, 132501 (2007).
[22] T. Ohnishi et al., J. Phys. Soc. Jpn. **79**, 073201 (2010).
[23] K.-L. Kratz et al., Astrophys. J. **403**, 216 (1993).
[24] B. Pfeiffer et al., Z. Phys. A **357**, 235 (1997).
[25] A. Arcones and G. F. Bertsch, Phys. Rev. Lett. **108**, 151101 (2012).
[26] P. M. Walker and G. Dracoulis, Nature **399**, 35 (1999).
[27] R. F. Casten, Nucl. Phys. A **443**, 1 (1985).
[28] E. Bouchez et al., Phys. Rev. Lett. **90**, 082502 (2003).
[29] C. Chandler et al., Phys. Rev. C **56**, R2924 (1997).
[30] P. Möller, A. J. Sierk, R. Bengtsson, H. Sagawa, and T. Ichikawa, Phys. Rev. Lett. **103**, 212501 (2009).
[31] J. Hakala et al., Eur. Phys. J. A **47**, 129 (2011).
[32] S. Naimi et al., Phys. Rev. Lett. **105**, 032502 (2010).
[33] R. B. Cakirli and R. F. Casten, Phys. Rev. C **78**, 041301 (2008).
[34] J. A. Winger et al., Phys. Rev. Lett. **102**, 142502 (2009).
[35] M. Madurga et al., Phys. Rev. Lett. **109**, 112501 (2012).
[36] O. Arndt et al., Phys. Rev. C **84**, 061307(R) (2011).
[37] Y. Yano, Nucl. Instrum. Methods Phys. Res., Sect. B **261**, 1009 (2007).

[38] T. Kubo, Nucl. Instrum. Meth. B **204**, 97 (2003).
[39] T. Sumikama et al., Phys. Rev. Lett. **106**, 202501 (2011).
[40] H. Watanabe et al., Phys. Lett. B **696**, 185 (2011).
[41] S. Nishimura et al., Phys. Rev. Lett. **106** 052502 (2011).
[42] P. Möller et al., At. Data Nucl. Data Tables **66**, 131 (1997).
[43] P. Möller et al., Phys. Rev. C **67**, 055802 (2003).
[44] N. Nishimura et al., Phys. Rev. C **85**, 048801 (2012).
[45] N. Schunck et al., Phys. Rev. C **69**, 061305(R) (2004).
[46] C. B. Hinke, Ph.D. Thesis (2010).
[47] N. Uematsu and S. Nishimura, RIKEN Accel. Prog. Rep. **41**, 151 (2008).
[48] S. Nishimura, Nucl. Phys. News **22**, No. 3 (2012).
[49] M. Wilhelm et al., Nucl. Instrum. Meth. A **381**, 462 (1996).
[50] H. J. Wollersheim et al., Nucl. Instrum. Meth. A **537**, 637 (2005).
[51] P. H. Regan et al., Nucl. Phys. A **787**, 491c (2007).
[52] H. Watanabe et al., Phys. Lett. B **704**, 270 (2011).
[53] G. C. Ball et al., Phys. Rev. Lett. **86**, 1454 (2001).
[54] Z. H. Li et al., Phys. Rev. C **72**, 064327 (2006).
[55] H. Mach, R. L. Gill, and M. Moszyski, Nucl. Instrum. Meth. A **280**, 49 (1989).
[56] H. Mach et al., Eur. Phys. J. A **25**, 105 (2005).
[57] D. L. Smith et al., Phys. Rev. C **77**, 014308 (2008).
[58] M. Sawicka et al., Phys. Rev. C **68**, 044304 (2003).
[59] M. Famiano et al., Nucl. Instrum. Meth. A **496**, 248 (2003).
[60] S. Takeuchi et al., Phys. Rev. Lett. **109**, 182501 (2012).
[61] V. Tripathi et al., Phys. Rev. C **76**, 021301 (2007).
[62] S. Nishimura, AIP Conf. Proc. **1269**, 91 (2010).
[63] K. Steiger et al., RIKEN Accel. Prog. Rep. **45**, (2012), in press.
[64] I. N. Borzov, Phys. Rev. C **71**, 065801 (2005).
[65] H. Schatz et al., Astrophys. J. **579**, 626 (2002).
[66] J. J. Cowan and C. Sneden, Nature **440**, 1151 (2006).
[67] I. U. Roederer et al., Astrophys. J. Lett. **747**, L8 (2012).
[68] M. R. Mumpower, G. C. McLaughlin, and R. Surman, Phys. Rev. C **86**, 035803 (2012).